The Astrophysical Journal, 943:14 (6pp), 2023 January 20 https://doi.org/10.3847/1538-4357/aca895

Energy Dependence of the Line Ratio $I(233.9\,\text{Å})/I(243.8\,\text{Å})$ in Fe XV Observed with an Electron Beam Ion Trap

Hiroyuki A. Sakaue[1], Daiji Kato[1,2], Norimasa Yamamoto[3], Izumi Murakami[1,4], Hirohisa Hara[5,6], and Nobuyuki Nakamura[7,1]
[1] National Institute for Fusion Science, Toki, Gifu 509-5292, Japan; sakaue.hiroyuki@nifs.ac.jp
[2] Interdisciplinary Graduate School of Engineering Sciences, Kyushu University, Fukuoka 816-8580, Japan
[3] Chubu University, Aichi 487-8501, Japan
[4] Department of Fusion Science, The Graduate University for Advanced Studies, SOKENDAI, Gifu 509-5292, Japan
[5] National Astronomical Observatory of Japan, Tokyo 181-8588, Japan
[6] Department of Astronomical Science, SOKENDAI, Tokyo 181-8588, Japan
[7] Institute for Laser Science, The University of Electro-Communications, Tokyo 182-8585, Japan
Received 2022 June 16; revised 2022 November 16; accepted 2022 December 1; published 2023 January 20

Abstract

We present the energy dependence of the intensity ratio between the $3s3p\ ^3P_2$—$3s3d\ ^3D_3$ transition at 233.9 Å and the $3s3p\ ^1P_1$—$3s3d\ ^1D_2$ transition at 243.8 Å in Fe XV studied with an electron beam ion trap over an energy range that spans resonance excitation regions. Clear resonance structures are observed in the electron energy range of 400–600 eV. The energy dependence obtained in the experiment is compared with a collisional-radiative model calculation, including resonance excitations, and overall agreement is found. It is shown that the ratio strongly reflects the population of the $3s3p\ ^3P_2$ metastable state, which is the lower state of the 233.9 Å transition.

Unified Astronomy Thesaurus concepts: Solar transition region (1532); Solar corona (1483); Solar flares (1496); Solar ultraviolet emission (1533); Solar atmosphere (1477); Stellar atmospheres (1584); Solar extreme ultraviolet emission (1493)

1. Introduction

Emission lines of highly charged Fe ions in the extreme-ultraviolet (EUV) range are very important for the spectroscopic diagnostics of the solar atmosphere, and thus have been observed with various devices such as the EUV Imaging Spectrometer (Culhane et al. 2007) on board the Hinode satellite, the Coronal Diagnostic Spectrometer (Harrison et al. 1995) on board the Solar and Heliospheric Observatory satellite, the Solar EUV Rocket Telescope and Spectrograph (Neupert et al. 1992), and so on. Fe XV is one of the most important ions for a temperature range of $\sim 2 \times 10^6$ K, and thus has been extensively studied hitherto. In the previous solar observations of the density sensitive ratio between the $3s3p\ ^3P_2$—$3s3d\ ^3D_3$ transition at 233.9 Å and the $3s3p\ ^1P_1$—$3s3d\ ^1D_2$ transition at 243.8 Å ($I(233.9)/I(243.8)$) in Fe XV, a deviation from calculations has often been reported (Dere et al. 1979; Dufton et al. 1990; Kastner & Bhatia 2001; Keenan et al. 2006). Dufton et al. (1990) suggested that the deviation is due to the unreliability of the theoretical values. On the other hand, Keenan et al. (2006) suggested that the inconsistency between the observation and the prediction was possibly caused by a blending of other lines, such as Ni XVIII at 233.8 Å and Ar XIV at 243.8 Å, and thus that the $I(233.9)/I(243.8)$ ratio is not suitable as a diagnostics measure, unless the spectral resolution is improved.

The $I(233.9)/I(243.8)$ ratio has also been studied in laboratories using an electron beam ion trap (EBIT; Nakamura et al. 2011; Shimizu et al. 2015; Tsuda et al. 2017). An EBIT plasma consists of trapped ions with a narrow charge state distribution and a quasi-monoenergetic electron beam; thus the emission spectra from an EBIT provide ideal benchmarks for plasma model calculations (Lepson et al. 2002; Ralchenko et al. 2006; Liang et al. 2009). Nakamura et al. (2011) and Shimizu et al. (2015) studied the electron density dependence of the $I(233.9)/I(243.8)$ ratio with the Tokyo-EBIT (Nakamura et al. 1997) and a compact EBIT called CoBIT (Nakamura et al. 2008), and found that the observed density dependence is rather stronger than that predicted by a collisional-radiative model (CRM) calculation, which results in poor agreement with the model for a higher density region. Although detailed comparison and discussion could not be made in those studies, as the sensitivity correction was not made, ratios obviously higher than the theoretically predicted high density limit (~0.7), e.g., values above unity were observed for some experimental conditions. It is noted that no significant blending of other lines affecting the ratio was found in their studies.

Tsuda et al. (2017) studied relative emission cross sections for the 233.9 and 243.8 Å lines as a function of electron energy, and found that the theoretical calculation with the fractional population, calculated with a CRM, underestimates the emission cross section of the 233.9 Å line for the electron energy region free from any resonance. It was suggested that the deviation is caused by an underestimation of the population of the $3s3p\ ^3P_2$ metastable state, which is the lower level of the 233.9 Å line, due to an error in the excitation cross section or the lifetime of the metastable state or both.

In this paper, we study the electron energy dependence of the $I(233.9)/I(243.8)$ ratio. The electron energy range covers resonance excitation via several autoionizing states in Fe XIV. The resonance excitation can affect the population of the $3s3p\ ^3P_2$ metastable state. The electron energy dependence of the population and its effect on the line ratio are studied through comparison with CRM calculations.

2. Experiment

The present experimental apparatus consisted of CoBIT and an EUV spectrometer (Nakamura et al. 2008; Sakaue et al. 2009). CoBIT is mainly composed of an electron gun, an ion trap (drift tube), an electron collector, and a superconducting coil installed inside a liquid nitrogen tank surrounding the ion trap. The superconducting coil is of a Helmholtz-like split type, which employs high critical temperature superconducting wires working at liquid nitrogen temperature. The electron beam emitted from the electron gun is accelerated (or decelerated) toward the ion trap while being compressed by the magnetic field produced by the superconducting coil. After passing through the ion trap, the electron beam is collected by the electron collector. Ions are trapped by a well potential (180 V by the present measurements) applied to the drift tube and the space charge of the compressed electron beam. Highly charged ions are produced through successive electron impact ionization of the trapped ions. In the present experiments, a vapor of ferrocene ($Fe(C_5H_5)_2$) was injected through a gas injection system to produce Fe ions.

The EUV spectrometer used was of a flat-field grazing-incidence (87°) type with a 1200 grooves mm^{-1} laminar-type replica diffraction grating (30–002, Shimadzu Corporation). It was used in a slitless configuration because the source in CoBIT represented a line source with a width of several hundred microns. A back-illuminated extreme-ultraviolet sensitive charge-coupled device (CCD) detector was mounted at the focal position. The size of the CCD sensor was $26.8 \times 8.0\ mm^2$ with a pixel size of $20 \times 20\ \mu m^2$. The stray visible light from the cathode of the electron gun was filtered out by using a 0.15 μm thick aluminum foil, placed in front of the diffraction grating. The transmittance of the aluminum filter was larger than 80% for the wavelength range between 170 and 300 Å. The spectral resolution of the present arrangement was about 0.8 Å, which was mainly limited by the electron beamwidth, regarded as an entrance slit in the slitless configuration.

To obtain the electron energy dependence of the ratio, spectral observation was performed at about 50 energy values between about 410 and 570 eV. The interaction energy between the electrons and the trapped ions is determined by the potential difference between the electron gun cathode and the potential inside the ion trap, where the space charge potential of the electrons and the ions exist. Since it is generally difficult to estimate the space charge contributions, the electron energy was calibrated at the theoretical resonance energy peak value of 420 eV. 1 hr data accumulation was repeated three to four times at each electron energy for improving the statistics of the data. The trapped ions were dumped every 5 s to prevent heavy impurity ions from accumulating in the trap. The electron beam current was 10 mA throughout all the measurements.

3. Collisional-radiative Model

Emission line spectra were calculated using a CRM; 567 energy levels of Fe XV for the configurations of $2p^6 3(s, p, d)n'l'$ ($n' = 3$–7, $l' = 0$–4) are included in the present model. The energy levels and rates for electron impact excitation and deexcitation, electron impact ionization, and radiative decay via electric-dipole, quadruple-, and octapole- and magnetic-dipole, and quadruple transitions among these levels were calculated using HULLAC (Bar-Shalom et al. 2001). Table 1 shows the lowest 14 levels of the present CRM, comparing the excitation energies with those of the NIST database (Kramida et al. 2020).

Table 1
The Lowest 14 Energy Levels of Fe XV

Index	Configuration	Level	Energy (eV)	
			Present	NIST
1	$3s^2$	$^1S_0$	0	0
2	$3s3p$	$^3P_0$	28.899	28.9927
3	$3s3p$	$^3P_1$	29.628	29.7141
4	$3s3p$	$^3P_2$	31.368	31.4697
5	$3s3p$	$^1P_1$	44.141	43.6314
6	$3p^2$	$^3P_0$	69.081	68.7522
7	$3p^2$	$^1D_2$	69.478	69.3816
8	$3p^2$	$^3P_1$	70.292	70.0017
9	$3p^2$	$^3P_2$	72.378	72.1344
10	$3p^2$	$^1S_0$	82.550	81.7833
11	$3s3d$	$^3D_1$	84.335	84.1570
12	$3s3d$	$^3D_2$	84.462	84.2826
13	$3s3d$	$^3D_3$	84.654	84.4848
14	$3s3d$	$^1D_2$	95.339	94.4875

Note. Present results are obtained by HULLAC (Bar-Shalom et al. 2001). NIST stands for data from the NIST Atomic Spectra Database (Kramida et al. 2020).

Collision strengths were calculated using the distorted-wave approximation. Resonant excitation via autoionization states of Fe XIV: $2p^5 3s3l3l'n''l''$ (n', n'' = 3–5, l', $l'' \leqslant 4$) are included in the model. Each resonance strength was calculated separately and added to the distorted-wave collision strengths (isolate-resonance model approximation). The resonance profile was approximated by the Gaussian distribution function of FWHM = 4.5 eV so that the resonance profiles fit the experimental profiles.

4. Results and Discussion

Figure 1 shows a typical spectrum obtained at an electron energy of 460 eV. As indicated in the figure, three emission lines from Fe XV, listed in Table 2, were observed. Among them, the line at 284.2 Å is a resonance transition from the $3s3p\ ^1P_1$ excited state, as illustrated in Figure 2. On the other hand, the other two lines at 233.9 and 243.8 Å, whose ratio is of present interest, are transitions between excited states. The lower level of the 243.8 Å transition is the upper level of the prompt resonance transition with a probability of $\sim 2 \times 10^{10}$ s^{-1}. Thus there is practically no chance for the 243.8 Å transition to be excited back from the lower level ($3s3p\ ^1P_1$) even in a relatively high density plasma. On the other hand, the lower level of the 233.9 Å transition ($3s3p\ ^3P_2$) is a metastable state whose lifetime is predominantly determined by the magnetic-dipole transition rate to $3s3p\ ^3P_1$ to be about 25 ms. Thus the 233.9 Å transition has more chance to be excited back from the lower state as the electron density increases. This excitation mechanism, and thus the fractional population of the $3s3p\ ^3P_2$ metastable state, is important to determine the 233.9 Å transition intensity because the direct excitation from the ground state to the upper or lower levels has a small cross section as $\Delta J > 1$.

Another important mechanism to excite the upper or lower levels from the ground level is resonance excitation via dielectric capture to inner shell excited states in Fe XIV. For

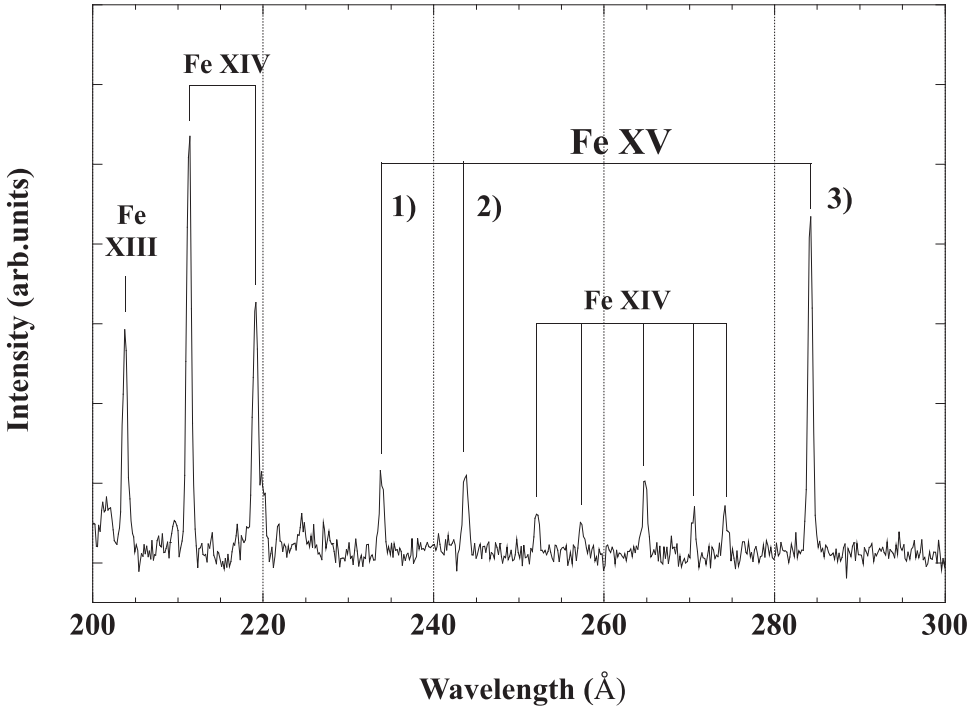

Figure 1. Typical Fe spectrum obtained with CoBIT at an electron energy of 460 eV.

Table 2
EUV Emission Lines in Fe XV Observed in the Present Study

Line Number	Transition				Wavelength (Å)
	Lower		Upper		
1)	$3s3p$	$^3P_2$	$3s3d$	$^3D_3$	233.865
2)	$3s3p$	$^1P_1$	$3s3d$	$^1D_2$	243.794
3)	$3s^2$	$^1S_0$	$3s3p$	$^1P_1$	284.164

example, at an electron energy around 420 eV, the following resonance excitation is possible.

$$\mathrm{Fe}^{14+}(2p^6 3s^2\ {}^1S_0) + \mathrm{e}^- \rightarrow \mathrm{Fe}^{13+}(2p^5 3s^2 3p3d) \rightarrow \begin{cases} \mathrm{Fe}^{14+}(2p^6 3s3p) + \mathrm{e}^- \\ \mathrm{Fe}^{14+}(2p^6 3s3d) + \mathrm{e}^-. \end{cases} \quad (1)$$

The energy dependence of the spectra in this energy range is shown in Figure 3. As seen in the figure, the relative intensity of the 233.9 Å transition showed a strong energy dependence, due to the above resonance excitation.

Figure 4(a) shows the electron energy dependence of the line intensity ratio between the 233.9 and 243.8 Å for the 410—570 eV region. It is noted that in the present experiment, the efficiency at 233.9 Å is considered to be higher than that at 243.8 Å by at least about 8%, considering the following three factors: (i) the transmittance of the aluminum filter, calculated assuming that it was pure aluminum, (ii) the CCD quantum efficiency supplied by the manufacturer, (iii) photon energy dependence of the photoelectron number in the CCD. In addition, the reflectivity of the grating should also slightly enhance the 233.9 Å intensity, although there is no quantitative data. The correction of 10% was thus applied to the ratio plotted in Figure 4(a). The solid blue line in Figure 4(a) shows the line ratio calculated by the present CRM. Since no emission lines from Fe XVI are seen in the observed spectrum (see Figure 1), Fe^{15+} is not considered in the present CRM. In Figure 4(a), calculated energy levels of the $2p^5 3s^2 3pnl$ and $2p^5 3s^2 3dnl$ intermediate states are also indicated by bars. In the energy region of 380 to 420 eV, resonant excitation via $2p^5 3s^2 3p3d$ is possible. In addition to the sharp resonance at 420 eV, which corresponds to Equation (1), broad and small resonance features are found at 450 eV and 550 eV, respectively. They correspond to the following Equations:

$$\mathrm{Fe}^{14+}(2p^6 3s^2\ {}^1S_0) + \mathrm{e}^- \rightarrow \mathrm{Fe}^{13+}(2p^5 3s^2 3d^2) \rightarrow \mathrm{Fe}^{14+}(2p^6 3s3d) + \mathrm{e}^- \quad \sim 450\ eV. \quad (2)$$

$$\mathrm{Fe}^{14+}(2p^6 3s^2\ {}^1S_0) + \mathrm{e}^- \rightarrow \mathrm{Fe}^{13+}(2p^5 3s^2 3p4l) \rightarrow \mathrm{Fe}^{14+}(2p^6 3s3p) + \mathrm{e}^- \quad \sim 550\ eV. \quad (3)$$

The sharp structure at 420 eV corresponds to the resonance excitation to $3s3d\ {}^3D_3$ via $[2p_{1/2}^{-1} 3s^2 3p_{1/2} 3d_{5/2}]_{J=5/2}$. As seen in the figure, although it seems that the model slightly underestimates the experiment, the overall features, including resonance structures, are in qualitative agreement. The ratio at $E_e = 500$ eV is about 0.55, which is consistent with the value obtained in the previous study with a similar experimental condition (500 eV, 10 mA) by Nakamura et al. (2011), although a higher ratio (∼0.9) was observed in the previous study at a higher electron current (15 mA). Figure 4(b) shows the calculated fractional population of the $3s3p\ {}^3P_2$. As seen in the figure, the fractional population shows strong energy dependence due to resonance excitation processes (1) to (3), in accord with the energy dependence of the $I(233.9)/I(243.8)$. The main population formation of $3s3d\ {}^3D_3$ and $3s3d\ {}^1D_2$, the upper levels of the 233.9 and 243.8 Å transitions, is thought to be due to the following four processes.

(i) Excitation from the lower levels, $3s3p\ {}^3P_2$ and $3s3p\ {}^1P_1$, respectively.
(ii) Collisional excitation from the ground state $3s^2\ {}^1S_0$ (including resonance excitation).

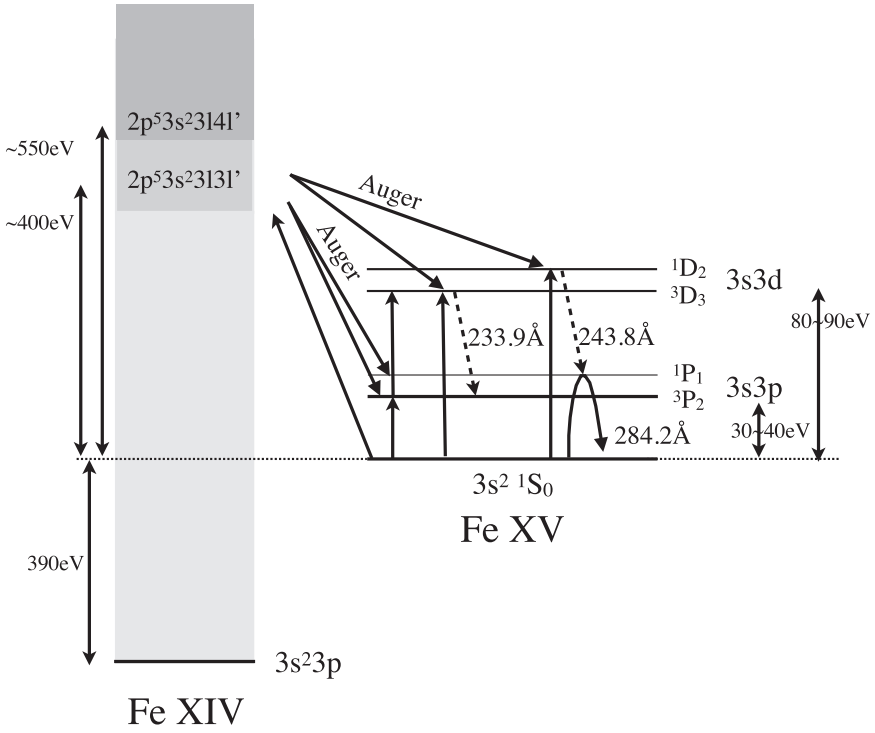

Figure 2. Energy diagram of Fe XIV and Fe XV.

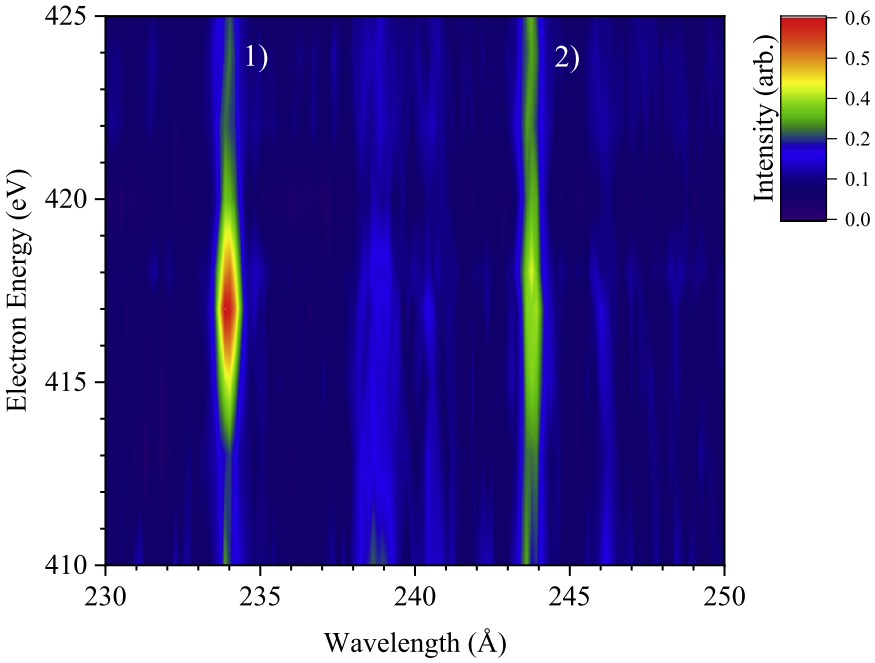

Figure 3. Energy dependence of Fe XV spectra in CoBIT. The color represents the intensity normalized to that of the 284.2 Å resonance transition.

(iii) Collisional excitations other than (i) and (ii).
(iv) Radiative decay from the excited level.

Figures 4(c) and (d) show the electron energy dependence of the in-flow rates into the $3s3d\ ^3D_3$ and $3s3d\ ^1D_2$ levels from CRM calculations, respectively. A large fraction of the in-flow rate into the upper level $3s3d\ ^3D_3$ of the 233.9 Å line is due to process (1), which is the excitation process from the lower level $3s3p\ ^3P_2$ (see Figure 4(c), blue line). Especially in the nonresonant energy region, its in-flow rate accounts for nearly 70% of the total. As shown in Figure 4(b), the metastable state of the $3s3p\ ^3P_2$ level has a large population, and the in-flow rate of the upper level is strongly reflected in its energy dependence. On the other hand, the in-flow rate into the upper level $3s3d\ ^1D_2$ state at 243.8 Å is mostly due to excitation from the ground state in process (2) (see Figure 4(d), green line). The in-flow rate from $3s3p\ ^1P_1$ in

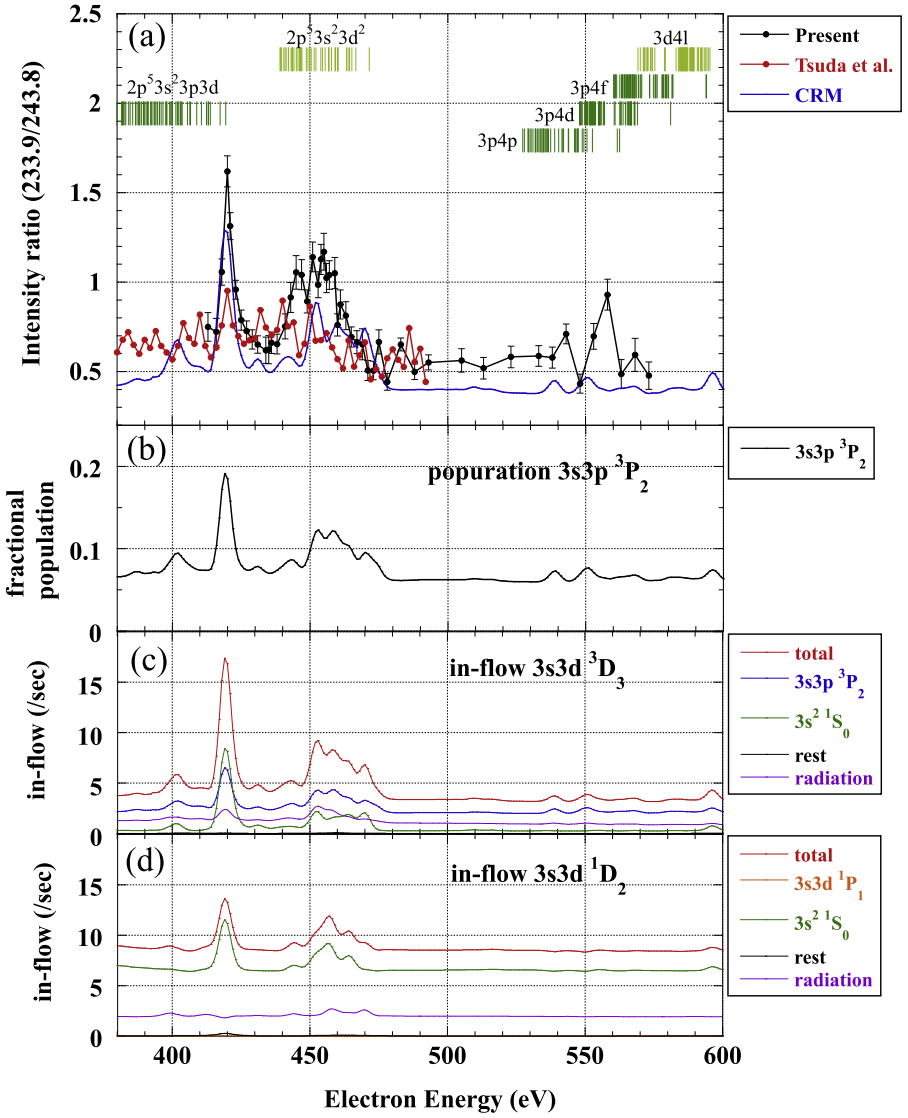

Figure 4. (a) Energy dependence of the $I(233.9)/I(243.8)$ ratio; black: present result; red: result of the fast sweep experiment by Tsuda et al. (2017); blue: collisional-radiative model (CRM) calculation. Calculated energy levels of the $2p^5 3s^2 3pnl$ and $2p^5 3s^2 3dnl$ intermediate states are also shown. (b) Calculated fractional population of the $3s3p\ ^3P_2$ state. (c) Calculated in-flow rate of the $3s3d\ ^3D_3$ state. (d) Calculated in-flow rate of the $3s3d\ ^1D_2$ state. Red: total in-flow rate; blue: excitation from $3s3p\ ^3P_2$; orange: excitation from $3s3p\ ^1P_1$; green: excitation from $3s^2\ ^1S_0$; black (rest): collisional in-flow rate from other than lower levels or ground states (without radiation processes); purple: radiative in-flow rate.

process (1) (at the orange color in Figure 4(d)) is zero and that (see Figures 4(c) and (d), black lines) in process (3) is negligibly small, while that (see Figure 4(d), purple line) in process (4) accounts for about 30% but does not show large energy dependence. Therefore, the energy dependence of the line ratios at 233.9 Å and 243.8 Å is strongly influenced by the metastable state of $3s3p\ ^3P_2$.

The electron energy dependence of the $I(233.9)/I(243.8)$ ratio was also measured by Tsuda et al. (2017). Different from the present measurements, they observed the ratio while sweeping the energy so rapidly (350 to 500 eV in 7 ms) that the population kept constant during the observation. Thus the ratio did not significantly change, as shown in Figure 4(a), in contrast to the present measurement. This is consistent with the fact that the energy dependence of the $3s3p\ ^3P_2$ metastable state population contributes strongly to the energy dependence of the $I(233.9)/I(243.8)$ ratio.

5. Summary

The line ratio $I(233.9)/I(243.8)$ of Fe XV has often been reported to deviate from calculations in previous solar observations, and there have been various arguments that the discrepancy is due to the unreliability of the theoretical value or to the blending of other emission lines. We explored the cause of the discrepancy, using laboratory plasmas, and pointed out that there is a discrepancy between the experimental and theoretical values, even if there is no emission line blending in the previous experiments. Extreme-ultraviolet spectra of Fe XV have been observed with an electron beam ion trap over a wide electron energy range. The observed line ratio between the 233.9 and 243.8 Å lines showed strong enhancement at some electron energy regions, due to resonance excitation processes. The enhancement has reasonably been reproduced by the collisional-radiative model calculations. The present experimental and theoretical results have shown that the population

of the $3s3p\ ^3P_2$ metastable state is important for the 233.9 Å line intensity, and thus for the ratio.

This work was supported by JSPS KAKENHI grant No. JP19H00665.

ORCID iDs

Hiroyuki A. Sakaue https://orcid.org/0000-0003-2209-3255
Daiji Kato https://orcid.org/0000-0002-5302-073X
Izumi Murakami https://orcid.org/0000-0001-7544-1773
Hirohisa Hara https://orcid.org/0000-0001-5686-3081
Nobuyuki Nakamura https://orcid.org/0000-0002-7009-0799

References

Bar-Shalom, A., Klapisch, M., & Oreg, J. 2001, JQSRT, 71, 169
Culhane, J. L., Harra, L. K., James, A. M., et al. 2007, SoPh, 243, 19
Dere, K. P., Mason, H. E., Widing, K. G., & Bhatia, A. K. 1979, ApJS, 40, 341
Dufton, P. L., Kingston, A. E., & Widing, K. G. 1990, ApJ, 353, 323
Harrison, R. A., Sawyer, E. C., Carter, M. K., et al. 1995, SoPh, 162, 233
Kastner, S. O., & Bhatia, A. K. 2001, ApJ, 553, 421
Keenan, F. P., Aggarwal, K. M., Bloomfield, D. S., Msezane, A. Z., & Widing, K. G. 2006, A&A, 449, 1203
Kramida, A., Ralchenko, Y., Reader, J. & NIST ASD Team 2020, Atomic Spectra Database v5.8, doi:10.18434/T4W30F
Lepson, J. K., Beiersdorfer, P., Brown, G. V., et al. 2002, ApJ, 578, 648
Liang, G. Y., Baumann, T. M., López-Urrutia, J. R. C., et al. 2009, ApJ, 696, 2275
Nakamura, N., Asada, J., Currell, F. J., et al. 1997, PhST, T73, 362
Nakamura, N., Kikuchi, H., Sakaue, H. A., & Watanabe, T. 2008, RScI, 79, 063104
Nakamura, N., Watanabe, E., Sakaue, H. A., et al. 2011, ApJ, 739, 17
Neupert, W. M., Epstein, G. L., Thomas, R. J., & Thompson, W. T. 1992, SoPh, 137, 87
Ralchenko, Y., Tan, J. N., Gillaspy, J. D., Pomeroy, J. M., & Silver, E. 2006, PhRvA, 74, 042514
Sakaue, H. A., Kato, D., Nakamura, N., et al. 2009, JPhCS, 163, 012020
Shimizu, E., Sakaue, H. A., Kato, D., et al. 2015, JPhCS, 583, 012019
Tsuda, T., Shimizu, E., Ali, S., et al. 2017, ApJ, 851, 82